

## RESEARCH ARTICLE

# Simplified automatic fault detection in wind turbine induction generators

Katharine Brigham<sup>ID</sup> | Donatella Zappalá<sup>ID</sup> | Christopher J. Crabtree<sup>ID</sup> |  
Christopher Donaghy-Spargo<sup>ID</sup>

Department of Engineering, Durham  
University, Durham, UK

**Correspondence**

Katharine Brigham, Department of  
Engineering, Durham University, Durham, UK.  
Email: katharine.g.brigham@durham.ac.uk

**Present Address**

Katharine Brigham, South Road, Durham  
DH1 3LE, UK

**Funding information**

EPSRC SUPERGEN Wind Hub, Grant/Award  
Number: EP/L014106/1

**Abstract**

This paper presents a simplified automated fault detection scheme for wind turbine induction generators with rotor electrical asymmetries. Fault indicators developed in previous works have made use of the presence of significant spectral peaks in the upper sidebands of the supply frequency harmonics; however, the specific location of these peaks may shift depending on the wind turbine speed. As wind turbines tend to operate under variable speed conditions, it may be difficult to predict where these fault-related peaks will occur. To accommodate for variable speeds and resulting shifting frequency peak locations, previous works have introduced methods to identify or track the relevant frequencies, which necessitates an additional set of processing algorithms to locate these fault-related peaks prior to any fault analysis. In this work, a simplified method is proposed to instead bypass the issue of variable speed (and shifting frequency peaks) by introducing a set of bandpass filters that encompass the ranges in which the peaks are expected to occur. These filters are designed to capture the fault-related spectral information to train a classifier for automatic fault detection, regardless of the specific location of the peaks. Initial experimental results show that this approach is robust against variable speeds and further shows good generalizability in being able to detect faults at speeds and conditions that were not presented during training. After training and tuning the proposed fault detection system, the system was tested on “unseen” data and yielded a high classification accuracy of 97.4%, demonstrating the efficacy of the proposed approach.

**KEYWORDS**

automated detection, condition monitoring, fault detection, rotor electrical asymmetry, speed invariance

## 1 | INTRODUCTION

Reliable and efficient condition monitoring (CM) techniques play a crucial role in minimizing wind turbine (WT) operation and maintenance (O&M) costs for competitive development of offshore wind energy.<sup>1</sup> Current efforts in the wind industry are aimed at automating the data interpretation and improving the accuracy and the reliability of the diagnostic decisions to enable condition-based maintenance planning.<sup>2</sup> While alternatives are emerging, wound rotor induction generators (WRIGs), using a partially rated power converter connected to the rotor side, remain the most widely used machines in wind industry for medium- and large-size variable speed applications.<sup>3</sup> Reliability studies<sup>4-7</sup> have reported that generator faults contribute significantly to WT downtime. Rotor electrical asymmetry, caused by brush-gear degradation, slip-ring wear/faults, or winding electrical faults, has been identified as one of the main contributors to WT generator failure rate.<sup>8,9</sup> Undetected generator faults may have a catastrophic effect on the turbine drive train resulting in costly repairs and long downtimes. Attention at the incipient fault stage is required to avoid fault escalation leading to breakdown.

Diagnosis methods to detect WRIG rotor failures, on the basis of time domain and/or frequency domain techniques, have been researched extensively. Motor current signature analysis (MCSA) is a well-established signal-based technique, typically using noninvasive, spectral-based

This is an open access article under the terms of the Creative Commons Attribution License, which permits use, distribution and reproduction in any medium, provided the original work is properly cited.

© 2020 The Authors. Wind Energy published by John Wiley & Sons Ltd

machine terminal quantity analysis, for detecting induction machine faults.<sup>10-12</sup> Stator current is commonly used in MCSA since it is sensitive to the rotor faults, and it is a suitable method to obtain a diagnostic index allowing the discrimination between faulty and healthy conditions.<sup>13</sup> Rotor asymmetry has been shown to induce a change in the generator stator current spectral content at slip-dependent sidebands of the dominant supply frequency harmonic components. Closed-form analytical expressions have been derived as to the specific locations of these sidebands<sup>11,14-18</sup> that can be monitored for diagnostic purposes for machine operating in steady state. MCSA was expansively investigated for rotor asymmetry detection in WRIGs under steady-state conditions, ranging from analysis of experimental data only<sup>19,20</sup> to investigation on the basis of both simulation and experimental data.<sup>21-23</sup>

In the WT industry, electrical signal-based CM has been gaining increasing attention, as it requires almost no additional capital expenditure.<sup>24</sup> This is due to the fact that electrical signals are already available in existing WT control and protection systems, and no additional sensors or data acquisition devices are needed. However, despite the increasing concern about WT electrical component reliability and growing attention in electrical signal-based CM, monitoring generator electrical faults has not yet become standard practice in the wind industry. The majority of WT CM systems (CMS) are mainly based on monitoring high-frequency vibration in gearbox and generator bearings.<sup>25</sup> In WT time-varying operating conditions, as the speed and then the slip changes, the frequency components associated with rotor faults are spread in a frequency range proportional to the operational speed variation range. This represents one of the main limitations associated to the effective implementation of MCSA techniques for WT generator CM as accurate information about the machine speed and specialist knowledge, with advanced signal analytics experience, are required to interpret large amounts of complex monitoring data.<sup>3</sup> Further to this, if the machine speed is unknown, it may not be possible to predict where these fault-related peaks will occur. In order to achieve a good spectral resolution, signal should be also sampled at high sampling rates, requiring large memory space for data storage and processing. To use CM information successfully for optimizing the O&M strategies, systems that can automatically analyse and interpret large volumes of CM data are required.

Recent works have dealt with the problem of WRIG rotor fault detection under nonstationary conditions. Gritli *et al*<sup>26</sup> and Vedreño *et al*<sup>27</sup> proposed approaches on the basis of detecting the faults through increases in signal energy in specific frequency ranges, including the fault component of interest. However, they rely on the use of the computationally intensive discrete wavelet transform (DWT) as filtering tool to isolate frequency intervals of interest and require the knowledge of the machine speed to identify in which band of the DWT decomposition the fault components appear. The harmonic order tracking analysis method presented by Sapena-Bano *et al*<sup>28</sup> rearranges the information in the current time-frequency spectrograms into simplified graphs displaying a unique pattern for each type of fault. However, this methodology strictly relies on the knowledge of the rotor position in every sampling time, which is usually not available on operational WTs. All these approaches, besides requiring the knowledge of the machine speed or rotor position, imply complex additional calculations to characterize the machine fault signatures for every machine operating condition. This makes their industrial implementation difficult.

This paper proposes an automated fault detector of WT induction generator rotor electrical asymmetry that requires minimal prior knowledge of the machine operating conditions and is invariant to the issue of shifting slip-dependent fault-related peaks in the stator current spectral content. Building on previous research,<sup>14,16,17,20,23</sup> the proposed method is a simplified but effective approach that negates the need for supplementary processing to identify operational parameters and is based on the combination of simplified signal processing tools for feature extraction from the machine stator current signal and the use of a linear classifier for fault detection. Unlike previous works on artificial intelligence (AI)-based algorithms for automatic induction motor fault detection, such as Fernandez-Temprano *et al*, Frosini *et al*, and Haroun *et al*<sup>29-31</sup> and those reviewed in Riera-Guasp *et al*,<sup>12</sup> tested under machine steady-state conditions, this work has been specifically developed to improve the fault diagnostic reliability during WT nonstationary load and speed operating conditions.

In general, the approach for developing an automated detection/classification system is to first extract a set of features from input data (eg, images and speech signals) and then use these features to train a classifier.<sup>32</sup> Subsequent data can then be classified by applying the same feature extraction approach and then inputting the features into the previously trained classifier to arrive at a decision about the class of the input data (eg, healthy or faulty), or even a categorization of the level of the fault severity, if a fault exists. The selection of an appropriate set of features is undoubtedly critical in this process towards implementing a successful detection system, as it is possible to extract features that do not contain information relevant for classification. Therefore, the suitability of the proposed set of features for automated fault detection is also investigated in this work, by applying a form of supervised dimensionality reduction to allow for both visual and numerical analyses of experimental healthy and faulty data. The applicability of the proposed approach to detecting different fault levels is experimentally validated in a laboratory test rig.

The main advantages of the proposed method are

1. It does not require any speed measurement, and it has been experimentally validated under stationary and wind-like variable speed conditions.
2. It allows automatic classification of the WT generator condition without requiring expert knowledge in signal processing, significantly reducing the large degree of manual analysis currently required and facilitating reliable diagnostics.
3. It allows fault severity discrimination providing early generator rotor damage detection warnings as part of a predictive maintenance regime.
4. It can be easily adapted to existing integrated monitoring systems and applied remotely to automatically monitor WT electrical signatures.

## 2 | PROPOSED METHODOLOGY

Previous work<sup>14,17</sup> has shown that WRIG rotor electrical asymmetry gives rise to additional frequency components in the stator current at characteristic slip-dependant frequencies,  $f^k$ , given by:

$$f^k = \left| j \pm \frac{k}{p}(1-s) \right| f, \quad (1)$$

where  $f$  is the fundamental supply frequency,  $s$  is the induction generator fractional slip,  $p$  is the machine pole pair number,  $k = 0, 1, 2, 3, \dots$ , and  $j = 0, 1, 2, 3, \dots$  relate to air-gap field space harmonics resulting from the layout of the machine and supply time harmonics in the current, respectively.

Given these findings regarding the manifestation of significant spectral peaks due to rotor asymmetry and the variability of the peak locations with the machine operating speed, the extracted features should incorporate information across the various frequency bands of interest. To this end, a set of bandpass filters is proposed (hereafter referred to as a filter bank), where the cut-off frequencies of the bandpass filters are determined on the basis of an expected range of slip-dependent sideband peak locations, derived from both theory and actual experimentation. The average spectral magnitude contained in each frequency band of the filter bank is computed and concatenated to form a vector of features, whose length is equal to the number of bandpass filters.

With the introduction of these bandpass filters, any fault-related information contained within the frequency bands of interest can be found without the need for any frequency tracking or identification of the relevant spectral components. Each bandpass filter is expected to cover the range of where the relevant spectral peaks occur, and taking the average magnitude in each band reduces the spectral content contained in that range to a single metric in which the fault-related information is naturally captured. These metrics, which will be used as the “features,” can then be combined (ie, concatenated) for usage in automatic classification.

## 2.1 | Feature extraction

The mathematics for computing the features from the input signals are as follows. First, the frequency domain representation of the stator current signature is computed by taking the Discrete Fourier Transform (DFT) over a windowed data vector  $\mathbf{x}_w[n] = \mathbf{h}[n] \odot \mathbf{x}[n]$ , where  $\mathbf{h}[n]$  is a windowing function (eg, a Hamming window), and  $\mathbf{x}[n]$  is the original data sample vector sampled at frequency  $f_s$  (Hz) over a window sample time of  $N_w$  (seconds).

For all data, the features are extracted using a filter bank approach on the stator current spectra whereby a set of  $R$  bandpass filters,  $H_r$  for  $r = 1, \dots, R$ , are applied (ie, multiplied by the spectrum). Each filter encompasses a frequency band of range  $f_{r,\text{range}} = f_{r,\text{max}} - f_{r,\text{min}}$ , which can discretely be represented as

$$H_r[k] = \begin{cases} 1, & k = \lfloor f_{r,\text{min}} \cdot (N/f_s) \rfloor, \dots, \lfloor f_{r,\text{max}} \cdot (N/f_s) \rfloor \\ 0, & \text{otherwise} \end{cases} \quad (2)$$

where  $f_{r,\text{min}}$  and  $f_{r,\text{max}}$  are the lower and upper cut-off frequencies, respectively, for the  $r^{\text{th}}$  bandpass filter;  $N$  is the length of the signal being analysed, where  $N \geq N_w \cdot f_s$  (with the inequality accounting for optional zero-padding), and  $k \in \mathbb{N}$ . Application of these bandpass filters is essentially an extraction of the spectral content in the frequency range of interest (ie, zeroing out the spectral content outside of the range of the bandpass filter, while “passing,” or multiplying by 1, the spectral content contained within the range of the bandpass filter). Different stator current bandpass filters are constructed under the guidance of work done by Zappalá,<sup>34</sup> which states that in faulty spectra (compared with “healthy” spectra), higher amplitude peaks will appear at the  $2sf$  upper sidebands of the supply frequency harmonics  $hf$ , where  $h = 1, 2, 3, \dots$  is the supply harmonic order. Therefore the filter bank will be constructed such that each bandpass filter encompasses this  $2sf$  upper sideband of each supply frequency harmonic order  $h$ :

$$f_{r,\text{min}} = hf + f_{\text{shift}}, \text{ and} \quad (3)$$

$$f_{r,\text{max}} = hf + f_{\text{shift}} + f_{\text{range}}, \quad (4)$$

where  $f_{\text{shift}}$  marks the start of the bandpass filter. The frequency range containing the sideband peaks,  $f_{\text{range}}$ , can be computed from the expected machine operational speed range. Note that while there could be an equivalence of  $r \equiv h$  if there is a filter for each harmonic, in some cases it may not be necessary to have filters placed at each harmonic so that  $r \neq h$ .<sup>23</sup>

From the frequency spectra computed from each windowed signal, a feature vector,  $\mathbf{v}$ , will be constructed with each element in the vector  $\mathbf{v}[r]$  representing information from each bandpass filter and is generated by the following equation:

$$\mathbf{v}[r] = \frac{1}{k_2 - k_1 + 1} \sum_{k=k_1}^{k_2} X[k] H_r[k], \quad (5)$$

where  $k_1 = \lfloor f_{r,\text{min}} (N/f_s) \rfloor$  and  $k_2 = \lfloor f_{r,\text{max}} (N/f_s) \rfloor$  (ie, the start and stop indices of the range in which the filter is nonzero), and  $\mathbf{v}[r] \in \mathfrak{R}^R$ . A flowchart of this proposed feature extraction approach is shown in Figure 1.

Note that there are several parameters that can be varied.

- Length of the analysis time window,  $N_w$ .
- Number of bandpass filters (interested harmonics),  $R$ .
- Frequency range of the bandpass filters,  $f_{\text{range}}$ .

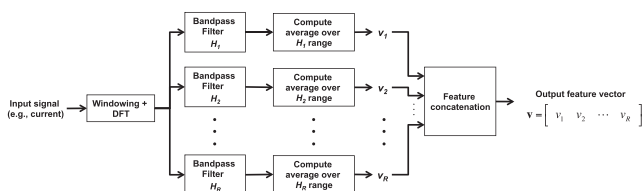


FIGURE 1 Feature Extraction Process

During experimentation, these parameters will be tuned (ie, the “best” values will be determined) by classifying the data using a held-out development set (not to be used in testing), in part to quantify the effects of these parameters on the resulting classifications.

## 2.2 | Dimensionality reduction and classification

To investigate the suitability of these features for automatic fault detection, Fisher linear discriminant (FLD) will be applied to the features since its usage permits visualization of the proposed features in a lower dimensional subspace and can help identify whether or not a distinct separation between healthy and faulty data can be attained. Note that although FLD is used and discussed herein, other popular classifiers such as support vector machines or artificial neural networks could also easily be applied, but the choice of classifier is not the primary focus of this work. FLD is merely used as a tool here to investigate the feasibility and demonstrate the efficacy of the proposed feature extraction approach. With FLD, the ability to achieve the desired distinctive separations can also be further analysed to determine whether or not such linear classifiers may be capable of detecting faults at multiple levels (eg, the fault detector should ideally be capable of detecting various levels of rotor imbalances). FLD further provides an added benefit of dimensionality reduction, as the application of FLD computes a linear function of the input data as follows:

$$\mathbf{y} = \mathbf{w}^T \mathbf{v}, \quad (6)$$

where  $\mathbf{y}$  is the (one dimensional) FLD output,  $\mathbf{w}$  is an  $R$ -dimensional weight (ie, projection) vector, and  $\mathbf{v}$  is an  $R$ -dimensional input vector (eg, a feature vector derived from an input data sample). The weight vector  $\mathbf{w}$  is determined using labelled “training” data to solve an optimization problem that minimizes the *within-class variability* (ie, spread of the data) and maximizes the *between-class separation* of the projected output data. A derivation of FLD will be described here to provide additional details on how FLD works.

Mathematical representations should first be defined for two quantities of interest: the *within-class variability* and the *between-class separation* of the resulting projected FLD outputs. While FLD has a multiclass variant,<sup>32</sup> for simplicity, the following description of FLD will be restricted to two classes. The within-class variability of the projected output from Equation (6) will be denoted as  $\mathbf{S}_k^p$  and can be defined as the total sample variance, which is given by<sup>32</sup>

$$\mathbf{S}_k^p = \sum_{n \in C_k} (\mathbf{y}_n - \mathbf{m}_k^p)^2, \quad (7)$$

where  $\mathbf{y}_n$  is the projected data point of the  $n^{\text{th}}$  input vector for  $n \in C_k$ , where  $C_k$  is the class and  $k = \{1, 2\}$  is the class index, and  $\mathbf{m}_k^p$  is the mean of the set of projected data points for class  $C_k$ .

The between-class separation of the projected data for classes  $C_1$  (ie, class 1) and  $C_2$  (ie, class 2) will be denoted as  $\mathbf{m}_{12}^p$  and can be defined as a distance between the means of the projected data from each class:

$$\mathbf{m}_{12}^p = (\mathbf{m}_1^p - \mathbf{m}_2^p)^2, \quad (8)$$

where  $\mathbf{m}_1^p$  and  $\mathbf{m}_2^p$  are the means of the projected data belonging to  $C_1$  and  $C_2$ , respectively, and are computed using their respective sample mean:

$$\mathbf{m}_k^p = \frac{1}{N_k} \sum_{n \in C_k} \mathbf{y}_n, \quad (9)$$

where  $N_k$  is the number of samples in class  $C_k$ . To both maximize the between-class separation and minimize the within-class variability, a ratio between the two measures can be constructed to formulate the following optimization function<sup>32</sup> for  $\mathbf{w}$ , the  $R$ -dimensional weight (ie, projection) vector:

$$J(\mathbf{w}) = \frac{(\mathbf{m}_1^p - \mathbf{m}_2^p)^2}{\mathbf{S}_1^p + \mathbf{S}_2^p}, \quad (10)$$

where  $\mathbf{S}_1^p$  and  $\mathbf{S}_2^p$  are the variances of the projected data belonging to classes  $C_1$  and  $C_2$ , respectively. The projected means and variances on the right-hand side of Equation (10) can be rewritten in terms of the original data and the weight vector  $\mathbf{w}$  (making the dependence of the function on the weight vector explicit) to obtain the following final form of the desired optimization function:

$$J(\mathbf{w}) = \frac{\mathbf{w}^T (\mathbf{m}_1 - \mathbf{m}_2) (\mathbf{m}_1 - \mathbf{m}_2)^T \mathbf{w}}{\mathbf{w}^T \mathbf{S}_W \mathbf{w}}, \quad (11)$$

where  $\mathbf{m}_1$  and  $\mathbf{m}_2$  are the sample means of the input data (feature vectors) and are given by

$$\mathbf{m}_k = \frac{1}{N_k} \sum_{n \in C_k} \mathbf{v}_n \text{ for } k = 1, 2, \quad (12)$$

where  $\mathbf{v}_n$  is from Equation (6) but explicitly for  $n \in C_k$ , and  $\mathbf{S}_W$  is the total *within-class* covariance:

$$\mathbf{S}_W = \sum_{n \in C_1} (\mathbf{v}_n - \mathbf{m}_1) (\mathbf{v}_n - \mathbf{m}_1)^T + \sum_{n \in C_2} (\mathbf{v}_n - \mathbf{m}_2) (\mathbf{v}_n - \mathbf{m}_2)^T. \quad (13)$$

Maximizing  $J(\mathbf{w})$  from Equation (11) with respect to  $\mathbf{w}$  results in the following closed-form solution for  $\mathbf{w}$ <sup>32</sup>:

$$\mathbf{w} = \mathbf{S}_W^{-1} (\mathbf{m}_1 - \mathbf{m}_2). \quad (14)$$

An optimal threshold for separating the classes after applying Equation (6) to the input (ie, training) data using the weight vector  $w$  found from Equation (14) can subsequently be determined from the resulting input data projections.

### 2.3 | Experimental rig and data curation

The proposed approach was tested using data collected from a small-scale CM test rig used for WT drive train analysis. The rig was designed to act as a model for a WT drive train with the purpose of producing signals comparable with those encountered on an operational WT. It features a 54-kW direct current (DC) motor, operated as a prime mover and simulating the WT rotor input, driving an industrial four-pole, three-phase, 50-Hz, 30-kW WRIG. The WRIG is driven at either constant speed or nonstationary, variable speed conditions to reflect the stochastic effects of wind torque driving, via a commercial DC machine drive. A schematic diagram of this experimental facility is shown in Figure 2, and two photographs are shown in Figure 3.

Details of the test rig are given in Crabtree<sup>33</sup> and Zappalá.<sup>34</sup> Seeded-fault conditions can be induced or removed from the test rig drive train as required, enabling several electrical and mechanical faults to be implemented repeatedly on demand and under controlled driving conditions.

Rotor electrical asymmetry was simulated on the test rig WRIG by using a resistive load bank externally connected to the rotor circuit via the machine slip rings to vary the resistance into one rotor phase winding circuit. For experimental purposes, to represent the development of rotor electrical faults on an induction generator, such as brush-gear or slip-ring wear, two seeded-fault levels were implemented on the test rig by successively adding two additional external resistances of  $0.3\Omega$  and  $0.6\Omega$ , respectively, to phase 1 of the rotor circuit through the external load bank. The corresponding levels of rotor electrical asymmetry, given as a percentage of the rotor balanced phase resistance, were 21% and 43%, respectively. These values compare very favourably with other studies.<sup>17,21</sup>

Data was collected at both steady-state speeds, ranging from 1520 to 1600 rpm and at wind-like variable speeds. In each constant speed test, the rig was driven for 300 seconds, while in each variable speed test, it was driven for 450 seconds to allow for sufficient data acquisition. Variable speed machine testing was performed according to speed profiles derived from a 2-MW variable speed WT model. This model, developed by the

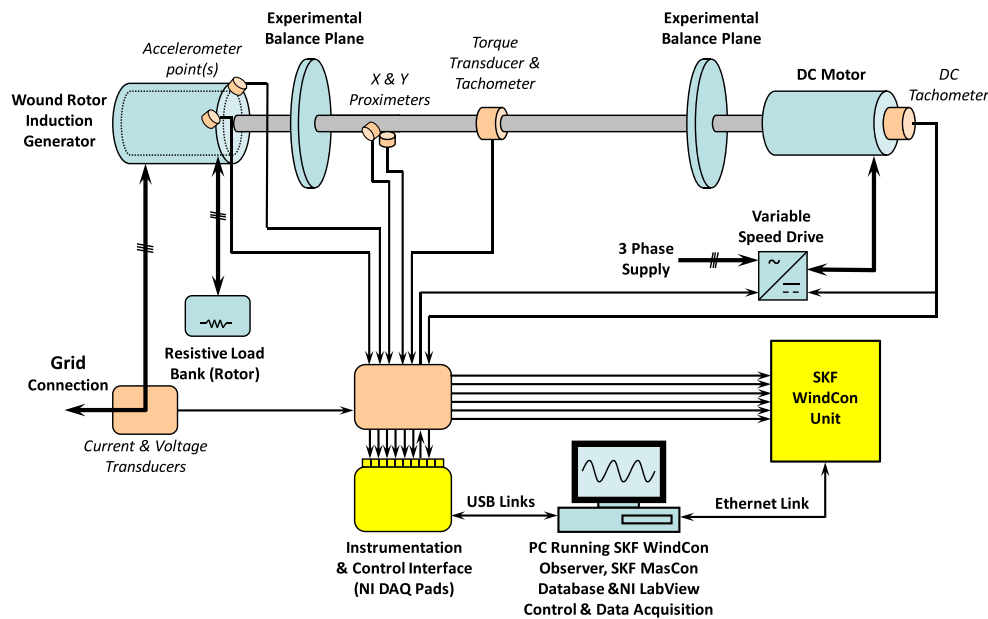


**FIGURE 2** Schematic diagram of the wind turbine condition monitoring test rig<sup>34</sup> [Colour figure can be viewed at [wileyonlinelibrary.com](http://wileyonlinelibrary.com)]

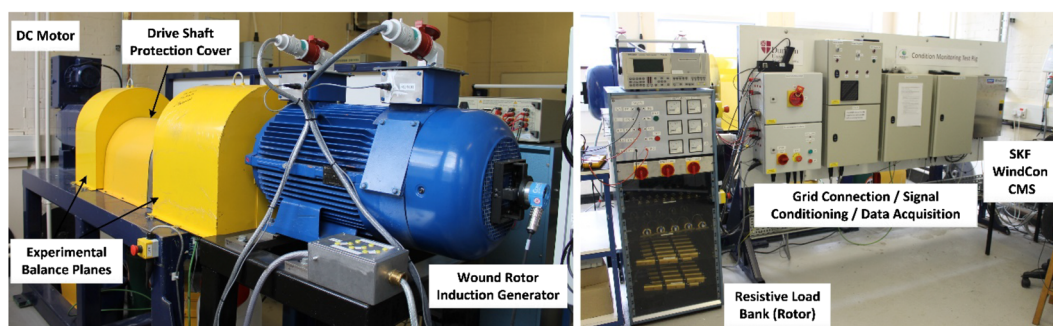


**FIGURE 3** Wind turbine condition monitoring test rig: main components, instrumentation, and control systems<sup>34</sup> [Colour figure can be viewed at [wileyonlinelibrary.com](http://wileyonlinelibrary.com)]

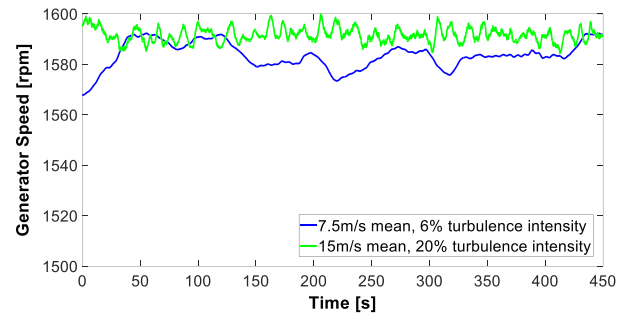


**FIGURE 4** Wind turbine condition monitoring test rig variable speed test conditions<sup>34</sup> [Colour figure can be viewed at [wileyonlinelibrary.com](http://wileyonlinelibrary.com)]

University of Strathclyde, as part of the SUPERGEN Wind Energy Technologies Consortium, incorporates the properties of natural wind and the mechanical behaviour of a 2-MW variable speed WT operating under closed-loop conditions.<sup>33</sup>

A variety of wind speeds and turbulence intensities, defined as the measure of the overall level of turbulence,<sup>35</sup> was applied to the model. The driving conditions were then scaled to the test rig on the basis of the generator speed data from the model as described in detail in Crabtree.<sup>33</sup> The use of the 2-MW variable speed WT driving model has allowed the simulation of the different dynamic speed behaviours that a full-size WT four-pole double-fed induction generator (DFIG) exhibits both below and above rated wind speed. The scaled generator variable speed signals used for testing, shown in Figure 4, are:

1. 7.5 m/s mean, 6% turbulence intensity, representative of a low mean wind speed with low turbulence, with the WT operating at or below rated wind speed under generator speed control (hereafter denoted as “7.5m6t”).
2. 15 m/s mean, 20% turbulence intensity, representative of a high mean wind speed with high turbulence, with the WT operating above rated wind speed under blade pitch control (hereafter denoted as “15m20t”).

Three-phase generator stator terminal voltages and currents are measured using transducer boards with a bandwidth of DC-100 K Hz. A Magtrol TMB 313/431 torque transducer, capable of outputting 60 pulses per revolution, is used measure the shaft torque but also as shaft pulse tachometer. The signal acquisition is performed using an NI 6015 data acquisition pad at a rate of 5 kHz. The pad is in turn connected via shielded universal serial bus (USB) connection to the NI LabVIEW environment that also operates as control environment of the rig. Only one line current signal is presented and analysed here, as is usually the case for MCSA.<sup>33</sup>

Three main sets of experimental data were curated and processed in this work that encompass a set of constant speeds spread across the experimental range and also include variable speed data. Table 1 shows the details of each experimental data set. *TrainSet* is used to train FLD, *DevSet* is used to determine reasonable feature extraction parameters using the trained FLD weight vector, and *EvalSet* is used to test the final fault detection system. Note that *EvalSet* is never used during training or “development” phase (during which the system parameters are tuned); the idea is that at least one data set should be held out to test the generalizability of the proposed detection system (ie, how does the detection system perform on never-before-seen data). Also of note is that during training, only the “healthy” and “21% rotor asymmetry” data are used. This is to test how well the proposed fault detector can distinguish between different levels of fault (eg, “43% rotor asymmetry”) even when the different fault levels are not present in the training data.

The above data sets are curated in a way to demonstrate the robustness of the scheme against different and variable speeds (ie, to demonstrate the speed invariance of the proposed scheme). The training data set only contains one set of data collected at a single, constant speed, yet the approach is tested on five to six other sets of data (within the *DevSet* and *EvalSet*) that are collected at other speeds that are not contained in the training set and also include variable speed data.

**TABLE 1** Speed and fault level details for the three curated data sets

Data set	Speed, rpm	Fault Level
TrainSet	1520	None (healthy)
		21% rotor asymmetry
DevSet	1525	
	1540	
	1553	
	1585	
	1600	None (healthy)
	Variable (7.5m6t)	21% rotor asymmetry
EvalSet	1530	43% rotor asymmetry
	1555	
	1565	
	1590	
	variable (15m20t)	



### 3 | RESULTS AND DISCUSSION

A single line current stator signal has been used in the study of the proposed approach to WRIG fault detection. With an expected range of speeds between 1520 and 1600 rpm, each bandpass filter was designed to start at each supply frequency harmonic +1 Hz (ie, for this set of experimental data,  $f_{\text{shift}} = 1$  Hz) and has an  $f_{\text{range}}$  of 7 Hz to capture the upper sideband. The number of bandpass filters used was initially (arbitrarily) selected to be 10 (ie, one filter is placed at the upper sideband of the 1st through 10th supply frequency harmonics), along with a time window of  $N_w = 10$  s.

After extracting the proposed set of features and training the classifier, the training data (ie,  $\text{TrainSet}$ ) was projected to determine an appropriate threshold for classifying “healthy” and “faulty,” which was selected as the halfway point between the means of each projected class. Numerical measures of the system performance were taken to be the system accuracy (ie, the percentage of correctly identified samples) and the false positive rate (FPR) (ie, the false “alarm” rate), which is computed as the number of “healthy” samples incorrectly categorized as “faulty” over the total number of samples that was determined to be “faulty.” The FPR is reported in addition to the system accuracy, as it is an important measure in health monitoring, since declaring a fault when the system is healthy would likely result in unnecessary expenditure of time and money to investigate a non-issue, and the FPR should be extremely low. The resulting classifications for the  $\text{DevSet}$  (categorizing both “21%” and “43%” as faulty) are shown in Table 2 for the initially selected feature extraction parameters.

The initial system accuracy and the FPR show the efficacy of the proposed solution in detecting faults in the stator current spectra as the resulting accuracy is quite high with a low FPR. In addition, this approach was coded and timed in MATLAB, and the average processing time to determine system health (ie, healthy or faulty) for one 10-second window of data, at a sampling frequency of 5 kHz, was 9.4 ms. This time includes extracting a set of features and classification, so in addition to high accuracy, there is also very little computational cost required.

It may also be possible to achieve better system performance by “tuning” the feature extraction parameters described in Section 2.1. Tables 3–5 show the system performance results for varying the length of the time window, the number of bandpass filters, and the frequency range of the bandpass filters, respectively.

Note that in Table 5, the lower cut-off frequency (ie, the supply harmonic +1 Hz) is the same for all frequency ranges; it is only the higher cut-off frequency that is varied. For the other parameters,

- In Table 3, 10 bandpass filters were used with a frequency range of 7 Hz each (ie, initially selected feature extraction parameters).
- In Table 4, a 7-second time window was used, as this yielded a “best” result shown in Table 3, and each filter had a frequency range of 7 Hz.
- In Table 5, a 7-second time window was used with 20 bandpass filters, as this yielded a “best” result shown in Table 4.

The results shown in Tables 3 through 5 show that (1) longer time windows yield more accurate results, which is to be expected as better spectral estimates are obtained with more data; (2) adding more filters (ie, generating more features) helps but having too many filters (in the

Feature Extraction		Accuracy	False Positive Rate (FPR)
Parameter	Value		
Time window	10 s		
Number of filters	10	98.8%	1.2%
Freq. range	7 Hz		

**TABLE 2**  $\text{DevSet}$  accuracy and false positive rate (FPR) for the initial set of feature extraction parameters

Feature Extraction		Accuracy	False Positive Rate (FPR)
Parameter	Value		
Time window	1 s	76.6%	24.6%
	3 s	75.3%	5.9%
	4 s	83.2%	5.1%
	5 s	98.8%	1.5%
	7 s	98.8%	1.1%
	10 s	98.8%	1.2%

**TABLE 3**  $\text{DevSet}$  accuracy and false positive rate (FPR) when varying the length of the time window

Feature Extraction		Accuracy	False Positive Rate (FPR)
Parameter	Value		
Number of filters	1	81.6%	21.7%
	2	84.7%	18.7%
	5	96.2%	5.4%
	7	96.6%	2.0%
	10	98.8%	1.1%
	15	98.8%	1.1%
	20	99.4%	0.9%
	25	85.8%	1.4%

**TABLE 4**  $\text{DevSet}$  accuracy and false positive rate (FPR) when varying the number of bandpass filters

**TABLE 5** DevSet accuracy and false positive rate (FPR) when varying the frequency range of the bandpass filters

Feature Extraction		Accuracy	False Positive Rate (FPR)
Parameter	Value		
Freq. range	5 Hz	69.2%	7.3%
	7 Hz	99.4%	0.9%
	9 Hz	89.8%	8.0%

case of 25 filters) results in lower accuracy—it is likely that at much higher order harmonics, there is not much additional information (more noise) that negatively impacts the ability to discriminate; and (3) the frequency range of the bandpass filters can significantly impact the classification rate. As for the last point regarding the filter frequency range, this should be selected on the basis of on the expected range of machine speeds in order to include relevant slip-dependent fault indicators. Too small of a range will miss capturing fault information, but too large of a range (beyond the expected range of speeds) may include too much noise. This range should be set dependent on the field equipment specifications, but further studies can be done to study the effects of applying noise reduction techniques on the spectra to allow for wider frequency ranges.

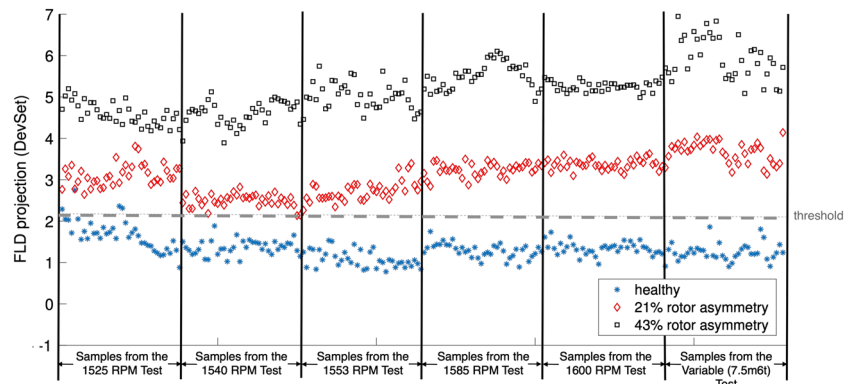
The resulting FLD projections for the DevSet are shown in Figure 5.

These features were extracted using a 7-second time window and 20 bandpass filters with a frequency range of 7 Hz. A clear delineation between the healthy and faulty data can be seen. Of interest is also the faulty data with 43% rotor asymmetry can be seen at even a different level (ie, range of projected values) compared with the “21% rotor asymmetry” data even though the “43%” data was not included during training. This result further highlights the potential of the proposed approach to be generalized to detect alternate fault levels beyond those present during training.

It should also clearly be noted that the final results presented on the DevSet are tuned (by varying the system parameters) so that better performance can be obtained. When there is a need or desire for tuning parameters, a typical approach in pattern recognition is to use cross validation<sup>32</sup> within the training set, where rotating portions of the training set are held out to test the various parameter settings. The parameters that yield the best system performance when tested on the held-out data are selected as the parameters that should be used on future test data. The approach used in this work follows this same concept, where the EvalSet can be considered the held-out portion, and the DevSet is used to tune the system parameters. This is also reflected in the naming of the curated data sets; the DevSet, or development set, is used to develop the system, and the EvalSet, or evaluation set, is used to evaluate the system. Therefore, without any further system tuning, using the “best” parameters found from the DevSet, the proposed approach was tested on the remaining held-out EvalSet. The EvalSet results are shown in Table 6, and the FLD projections for the EvalSet are shown in Figure 6.

The accuracy still remains relatively high with a 2% relative decrease in accuracy, although the FPR has a significant increase. It can be seen in Figure 6 that one particular set of test data included in the EvalSet (namely, the data on the left-hand side of Figure 6, which was collected at 1530 rpm) does not exhibit as much of a separation between classes as can be seen in the rest of the EvalSet data. It is possible that the data collected at this particular speed contain more noise than the others; future investigations may include noise-reduction techniques and further analyses on potential overfitting.

The proposed methodology can easily be scaled to the higher field WT power levels. WTs are monitored by commercial CMSs, and both electrical and mechanical signals are readily available to the operator, so no additional sensors/data acquisition systems would be required. Its application in the field would probably imply an increase in the spectral background noise because of the higher complexity of WT drive trains compared with the small-scale laboratory rig.

**FIGURE 5** Fisher linear discriminant (FLD) projection of the average spectral magnitudes of the stator current spectra computed in each bandpass filter for the DevSet containing speeds ranging from 1525–1600 rpm and a variable speed data set [Colour figure can be viewed at [wileyonlinelibrary.com](http://wileyonlinelibrary.com)]**TABLE 6** EvalSet accuracy and false positive rate (FPR) for the final selected set of feature extraction parameters

Feature Extraction		Accuracy	False Positive Rate (FPR)
Parameter	Value		
Time window	7 s		
Number of filters	20	97.4%	3.6%
Frequency range	7 Hz		



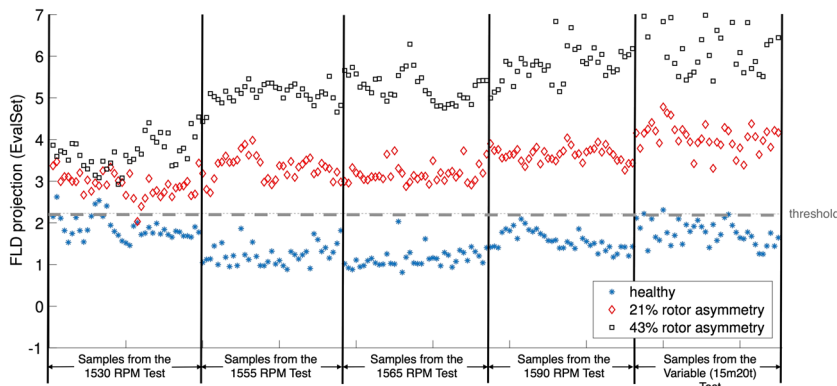


**FIGURE 6** Fisher linear discriminant (FLD) projection of the average spectral magnitudes of the stator current spectra computed in each bandpass filter for the EvalSet containing speeds ranging from 1530–1590 rpm and a variable speed data set [Colour figure can be viewed at [wileyonlinelibrary.com](http://wileyonlinelibrary.com)]

## 4 | CONCLUSIONS

This paper proposes an automated WT induction generator fault detector that requires very little training data, is robust against variable speeds, and achieves high accuracy at very little computational cost. The novelty of the approach includes a new way to analyse the data, in that other methods require frequency tracking or identification or conventional manual comparison of the spectra (as reported in previous works), but this method does not. The proposed methodology has been validated experimentally on a WT drive train test rig with two rotor fault levels under both constant and variable speed driving conditions, representative of WT generator field operation. The following specific conclusions arise:

- A set of bandpass filters is proposed to capture the stator current fault-related spectral information and to train a classifier, making the approach independent on the machine instantaneous speed.
- Unlike previous studies on the basis of the analysis of single speed-dependent fault-related frequencies in stator current, this work is more robust as it draws information from multiple frequency components into a single fault indicator.
- The proposed approach can provide clear differentiation between healthy and faulty conditions, under both constant and variable speed operating conditions, even though the classifier has been only trained on a single fault level and a single constant speed condition.
- Experimental results have initially shown clear discrimination between fault levels, with an almost linear response, even at variable speed. This suggests the ability of the proposed approach to provide early fault detection of developing damage, crucial for effective maintenance optimization.
- The developed method can be easily implemented into WT CMSs for efficient real-time analysis of data captured without requiring expert knowledge.

Future work in this area includes further investigations into the robustness of the proposed approach, including the impact of different training data (eg, training under variable speed conditions) on the ability to differentiate between different fault levels and healthy data. A comparative study using other classification approaches may also be undertaken as these different training conditions are explored.

## ACKNOWLEDGEMENT

This work was supported by the EPSRC SUPERGEN Wind Hub (grant EP/L014106/1). The data presented in this paper are available from the Durham Research Online Data Depository at <https://doi.org/10.15128/r2gq67jr17c>.

## ORCID

Katharine Brigham  <https://orcid.org/0000-0002-5398-5144>

Donatella Zappalá  <http://orcid.org/0000-0002-8283-5102>

Christopher J. Crabtree  <https://orcid.org/0000-0003-0109-5323>

Christopher Donaghy-Spargo  <https://orcid.org/0000-0001-5337-4522>

## REFERENCES

1. Qiao W, Lu D. A survey on wind turbine condition monitoring and fault diagnosis - part I: components and subsystems. *IEEE Trans Ind Electron.* 2015;62(10):6536–6545.
2. Crabtree CJ, Zappalá D, Hogg SI. Wind energy: UK experiences and offshore operational challenges. *Proc Inst Mech Eng A.* 2015;229(7):727–746.
3. Tavner PJ. Offshore wind turbines: reliability, availability and maintenance 1st ed.: IET Press; 2012.
4. Carroll J, McDonald A, McMillan D. Failure rate, repair time and unscheduled O&M cost analysis of offshore wind turbines. *Wind Energy.* 2016;19(6):1107–1119.
5. Tavner PJ, Faulstich S, Hahn B, van Bussel GJW. Reliability & availability of wind turbine electrical & electronic components. *EPE J.* 2010;20(4):45–50.

6. Wilkinson M, Harman K, Hendriks B. Measuring wind turbine reliability - results of the Reliawind project. In: Proc. Scientific Track of the European Wind Energy Association Conference; 2011; Brussel Belgium:1-8.
7. Artigao E, Martín-Martínez S, Honrubia-Escribano A, Gómez-Lázaro E. Wind turbine reliability: a comprehensive review towards effective condition monitoring development. *Appl Energy*. 2018;228:1569-1583.
8. Carroll J, McDonald A, Mcmillan D. Reliability comparison of wind turbines with DFIG and PMG drive trains. *IEEE Trans Energy Convers*. 2015;30(2):663-670.
9. Gritli Y, Rossi C, Casadei D, Filippetti F., Capolino G.-A. A diagnostic space vector-based index for rotor electrical fault detection in wound-rotor induction machines under speed transient. *IEEE Trans Ind Electron*. 2017;64(5):3892-3902.
10. El Hachemi Benbouzid M. Review of induction motors signature analysis as a medium for faults detection. *IEEE Trans Ind Electron*. 2000;47(5):984-993.
11. Tavner PJ, Ran L, Penman J, Sedding H. *Condition Monitoring of Rotating Electrical Machines*. 2nd ed. UK: IET Press; 2008.
12. Riera-Guasp M, Antonino-Daviu JA, Capolino GA. Advances in electrical machine, power electronic, and drive condition monitoring and fault detection: state of the art. *IEEE Trans Ind Electron*. 2015;62(3):1746-1759.
13. Henao H, Capolino GA, Fernandez-Cabanas M, Filippetti F, Bruzese C, Strangas E, Pusca R. Trends in fault diagnosis for electrical machines: a review of diagnostic techniques. *IEEE Ind Electron Mag*. 2014;8(2):31-42.
14. Williamson S, Djurovic S. Origins of stator current spectra in DFIGs with winding faults and excitation asymmetries. In: Proceeding IEEE International Electric Machines and Drives Conference, Miami, USA; 2009:563-570.
15. Gritli Y, Stefani A, Chatti A. The combined use of the instantaneous fault frequency evolution and frequency sliding for advanced rotor fault diagnosis in DFIM under time-varying condition.; 2009:3471-3476.
16. Djurovic S, Williamson S, Renfrew A. Dynamic model for doubly-fed induction machines with unbalanced excitation, both with and without winding faults. *IET Electr Power Appl*. 2009;3(3):171-177.
17. Djurovic S, Crabtree CJ, Tavner PJ, Smith AC. Condition monitoring of wind turbine induction generators with rotor electrical asymmetry. *IET Renewable Power Generation*. 2012;6(4):207-216.
18. Pilloni A, Pisano A, Riera-Guasp M. Fault Detection in induction motors. In: F Giri, ed. *AC Electric Motors Control: Advanced Design Techniques and Applications*. Hoboken, NJ: Wiley Press; 2013:275-309.
19. Vedreño-Santos F, Riera-Guasp M, Henao H, Pineda-Sanchez M, Puche-Panadero R. Diagnosis of rotor and stator asymmetries in wound-rotor induction machines under nonstationary operation through the instantaneous frequency. *IEEE Trans Ind Electron*. 2014;61(9):4247-4259.
20. Ibrahim R, Watson S, Djurovic S, Crabtree CJ. An effective approach for rotor electrical asymmetry detection in wind turbine DFIGs. *IEEE Trans Ind Electron*. 2018;65(11):8872-8881.
21. Stefani A, Yazidi A, Rossi C, Filippetti F, Casadei D, Capolino G-A. Doubly fed induction machines diagnosis based on signature analysis of rotor modulating signals. *IEEE Trans Ind Appl*. 2008;44(6):1711-1721.
22. Shah D, Nandi S, Netti P. Stator-interturn-fault detection of doubly fed induction generators using rotor-current and search-coil-voltage signature analysis. *IEEE Trans Ind Appl*. 2009;45(5):1831-1842.
23. Zappalá D, Sarma N, Djurovic S, Crabtree CJ, Mohammad A, Tavner PJ. Electrical & mechanical diagnostic indicators of wind turbine induction generator rotor faults. *Renew Energy*. 2019;131:14-24.
24. Yang W, Tavner PJ, Crabtree CJ, Feng Y, Qiu Y. Wind turbine condition monitoring: technical and commercial challenges. *Wind Energy*. 2014;17:673-693.
25. Crabtree CJ, Zappalá D, Tavner PJ. Survey of commercially available condition monitoring systems for wind turbines. Durham University and the SUPERGEN Wind Energy Technologies Consortium pp. 1-22; 2014.
26. Gritli Y, Zarri L, Rossi C, Filippetti F, Capolino G-A, Casadei D. Advanced diagnosis of electrical faults in wound-rotor induction machines. *IEEE Trans Ind Electron*. 2013;60(9):4012-4024.
27. Vedreño-Santos F, Riera-Guasp M, Henao H, Pineda-Sánchez M, Puche-Panadero R. Diagnosis of rotor and stator asymmetries in wound-rotor induction machines under nonstationary operation through the instantaneous frequency. *IEEE Trans Ind Electron*. 2014;61(9):4947-4959.
28. Sapena-Bano A, Burriel-Valencia J, Pineda-Sanchez M, Puche-Panadero R, Riera-Guasp M. The harmonic order tracking analysis method for the fault diagnosis in induction motors under time-varying conditions. *IEEE Trans Energy Convers*. 2017;32(1):244-256.
29. Fernandez-Temprano M, Gardel-Sotomayor PE, Duque-Perezet O. Broken bar condition monitoring of an induction motor under different supplies using a linear discriminant analysis. In: Proc. 9th IEEE International Symposium on Diagnostics for Electric Machines, Power Electronics and Drives (SDMPED), Valencia, Spain; 2013:162-168.
30. Frosini L, Zanazzo S, Beccarisi F. Linear discriminant analysis for an automatic detection of stator faults in induction motor drives. In: Proc. 11th IEEE International Symposium on Diagnostics for Electric Machines, Power Electronics and Drives (SDMPED), Tinos, Greece; 2017:503-509.
31. Haroun S, Nait Seghir A, Touati S. Multiple features extraction and selection for detection and classification of stator winding faults. *IET Electric Power Applications*. 2018;12(3):339-346.
32. Bishop CM. *Pattern Recognition and Machine Learning*. Berlin, Heidelberg: Springer-Verlag; 2006.
33. Crabtree CJ. Condition Monitoring Techniques for Wind Turbine. PhD thesis; 2011.
34. Zappalá D. Advanced Algorithms for Automatic Wind Turbine Condition Monitoring. PhD thesis; 2015.
35. Burton T, Sharpe D, Jenkins N. *Wind Energy Handbook*. 2nd ed: John Wiley & Sons; 2011.